

A Journal of the Gesellschaft Deutscher Chemiker

Angewandte Chemie

GDCh

International Edition

www.angewandte.org

Accepted Article

Title: Controlling Multiple Chiroptical Inversion in Biphasic Liquid-Crystalline Polymers

Authors: Wei Zhang, Xiaoxiao Cheng, Tengfei Miao, Yafei Ma, Xiaoyan Zhu, and Xiulin Zhu

This manuscript has been accepted after peer review and appears as an Accepted Article online prior to editing, proofing, and formal publication of the final Version of Record (VoR). This work is currently citable by using the Digital Object Identifier (DOI) given below. The VoR will be published online in Early View as soon as possible and may be different to this Accepted Article as a result of editing. Readers should obtain the VoR from the journal website shown below when it is published to ensure accuracy of information. The authors are responsible for the content of this Accepted Article.

To be cited as: *Angew. Chem. Int. Ed.* 10.1002/anie.202109084

Link to VoR: <https://doi.org/10.1002/anie.202109084>

Controlling Multiple Chiroptical Inversion in Biphasic Liquid-Crystalline Polymers

Xiaoxiao Cheng, Tengfei Miao, Yafei Ma, Xiaoyan Zhu, Wei Zhang* and Xiulin Zhu

Suzhou Key Laboratory of Macromolecular Design and Precision Synthesis, State and Local Joint Engineering Laboratory for Novel Functional Polymeric Materials, Jiangsu Engineering Laboratory of Novel Functional Polymeric Materials, College of Chemistry, Chemical Engineering and Materials Science, Soochow University
Suzhou, 215123 (China)
E-mail: weizhang@suda.edu.cn

Supporting information (including the Experimental Section) for this article is given via a link at the end of the document.

Abstract: While controlling the chirality and modulating the helicity is a challenging task, it attracts great research interest for better understanding the origin of chirality in nature. Herein, structurally similar azobenzene (Azo) vinyl monomers were designed in which the alkyl chains comprised the chiral stereocenter with different achiral tail lengths. Combining the synchronous polymerization, supramolecular stacking and self-assembly, multiple chiroptical inversion of the Azo-polymer supramolecular assemblies can be modulated by the tail length and DP of Azo blocks during in-situ polymerization. The DP-, UV light-, temperature-, aging time-dependent chiroptical properties and liquid-crystalline (LC) characterization indicated that the amorphous-to-LC phase transition and biphasic LC interconversion allows the transcription of intra-chain π - π stacking, inter-chain *H*- and *J*-aggregation, thereby controlling the dynamic multiple reversal of supramolecular chirality.

Control of the hierarchical chirality is the key to the complex biological processes in living organisms, which relies on a delicate balance between molecular, supramolecular and macroscopic chirality.^[1] To modulate the hierarchical chirality of intra- and/or inter-chain helical superstructures in polymer systems, key geometric parameters such as the topological shape, molecular weight distribution and stereochemistry are critical.^[2] Among main-chain helix in stiff rod-like polymers that exhibits "Sergeants-and-Soldiers Principle" and "Majority Rule", chiroptical inversion is a particularly intriguing phenomenon.^[3] The helicity of main-chain polymer backbone with low helix inversion barriers can be easily modulated by the chiral substituents in side chains. For supramolecular chirality in polymer systems, however, the dynamic chirality regulation and controlled helix inversion usually require external factors as the energetically demanding stimulus, such as solvent,^[4] light,^[5] dopant,^[6] temperature,^[7] and pH.^[8] In fact, the building blocks in supramolecules could self-organize in a controllable pathway through weak noncovalent interactions,^[9] therefore regulating the functionality-oriented stacking modes (*i.e.* intra- and inter-chain packing, *J*- and *H*-aggregation) of building blocks would be highly helpful to control the chiroptical properties of resulted nanostructures.^[10]

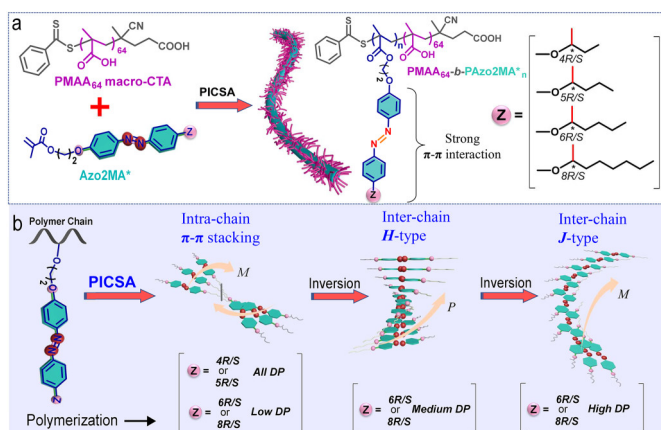
In general, polymeric supramolecular chiral assemblies are constructed through post-polymerization self-assembly method, which requires the synthesis of corresponding polymers before performing the assembly procedure.^[11] Nevertheless, such approach usually involves a multi-step process typically assembled at highly diluted conditions (usually <1 wt%). Fortunately, polymerization-induced self-assembly (PISA) can overcome these limitations by utilizing living polymerization

method to drive self-assembly in-situ. In the past few years, functional and templated PISA has been extensively investigated by Armes,^[12] Boyer,^[13] Pan,^[14] Chen^[15] and An^[16] et al. Recently, PISA was further employed for the precise and large-scale preparation of chiral block copolymer (BCP) assemblies in-situ. For example, Wan and O'Reilly et al. employed PISA strategy to prepare main-chain helical BCP assemblies with different morphologies including vesicles, lamellae and helical ribbons.^[17] We reported polymerization-induced chiral self-assembly (PICSA) as a universal platform for the construction of liquid-crystalline (LC) polymeric supramolecular assemblies.^[18] However, the underlying mechanism and factors determining the transcription of asymmetric tendency from molecular scale to supramolecular level and LC domain above, dynamic regulation of the pathway-dependent stacking mode and hierarchical chirality have not yet been well understood.^[19]

Azobenzene (Azo)-containing LC polymer has been reported to selectively form preferential helicity due to the synergistic and/or antagonistic Azo coupling between orientational order and asymmetric twist.^[20] It has also been proven that the micro-level phase transition can manipulate the the preferential helical superstructures.^[21] But little is known about the origin of the in-situ multiple chiroptical inversion in Azo supramolecular LC assemblies.^[22] The reasons are that it is challenge to construct supramolecular assemblies through a one-pot methodology at high concentrations and manipulate the supramolecular chirality in a controllable manner without external stimulus. Inspired by the above situation, we present an chirality control of Azo-polymer supramolecular assemblies by modifying achiral tail length of polymer side-chains, which exhibiting multiple polymerization-induced chiroptical inversion phenomena. These multiple chirality and helicity inversion were investigated and collectively confirmed to be mediated by the amorphous-LC phase transition, interconversion of stacking modes in bistable mesomorphism phase of Azo-polymers. The results suggested that chiroptical reversal in polymeric supramolecules can be independent of external stimulus and molecular configuration.

Herein, a series of chiral Azo monomers with different tail lengths but the stereogenic center maintained in the same position, *i.e.* adjacent to the aromatic core (Azo2MA*-m*R/S*, m is the number of carbon atoms in the tail, Scheme S1), were synthesized and confirmed to have high e.e. % values (Figure S1). The poly(methacrylic acid) macromolecular chain transfer agent (PMAA macro-CTA) was synthesized via reversible addition-fragmentation chain transfer (RAFT) solution

polymerization. The degree of polymerization (DP) of PMAA macro-CTA was 64, the M_n and \mathcal{D} were 11100 g/mol and 1.09, according to ^1H NMR spectra and GPC analysis (Figure S2), respectively. PMAA₆₄ macro-CTA was chain-extended with Azo2MA* in ethanol to produce a series of PMAA₆₄-b-PAzo2MA*_n BCP assemblies (2-*mR/S*, *m* = 4, 5, 6, 8, Scheme 1) at 70 °C by systematically tuning the target DP (DP = 5, 10, 20, 30, 40, 60) at 10% solid content. The RAFT-mediated PICSA followed typical two-stage kinetics with an obvious rate acceleration upon nucleation at 2 h, and nearquantitative monomer conversion was achieved at the end of polymerization (Figures S3-S5).



Scheme 1. a) Schematic presentation of polymerization-induced chiroptical inversion and chemical structures of the Azo-polymers. b) Proposed stacking modes within Azo-BCP supramolecular assemblies.

Upon synchronous polymerization, supramolecular stacking and self-assembly, the corresponding Azo-BCP supramolecular assemblies formed and showed aggregation-induced circular

dichroism (Figure 1) due to exciton coupling between interacted Azo units. The authenticity of the circular dichroism was confirmed by the negligible LD artifacts in the system (Figures S6 and S7). As shown in Figures 1a and 1b, when the alkyl tails of side-chain Azo-polymer assemblies are 4 and 5 (2-4*R/S*, 2-5*R/S*), all *S*-type supramolecular assemblies had a positive bisignate Cotton effect (signs are described referring to the longer wavelength of the extrema) and *R*-type counterparts had a negative effect. More importantly, all exciton couplets of the bisignate Cotton bands are centered at 320 nm, indicating the same type of chiral exciton coupling between Azo chromophores induced by aggregation (Agg1). When the alkyl tails are 6 and 8 (2-6*R/S*, 2-8*R/S*), a unique DP-dependent multiple chiroptical inversion effect was found for both tail lengths. For example, bisignate Cotton bands centered at 320 nm were also observed when the average DP is lower than 5 (Figures 1c and 1d), which can be classified as the formation of Agg1. As the DP of Azo blocks increased, the Cotton effects were inverted in nature (Figures 1e and 1f), indicating the opposite supramolecular chirality of assemblies, despite the fact that they have the same molecular configuration. In other words, *S*-type assemblies had a negative Cotton effect and *R*-type counterparts had a positive effect. Furthermore, two exciton couplets centered at 320 nm and 348 nm emerged when the DP = 10, where the former was attributed to the splitting of Agg1 and the new exciton coupling of the latter indicates the higher-order superstructures denoted as Agg2. Such triple CD signals indicated the formation of heterostructures within Azo-BCP assemblies involving multiple chiral excitons coupling of the transition-dipole moments. An increase in DP to 30 led to the disappearance of Agg1, and only the single exciton coupling induced by Agg2 existed (Figures 1e and 1f). Compared to the Cotton effects induced by Agg1, Agg2 with medium DP showed completely opposite CD signals.

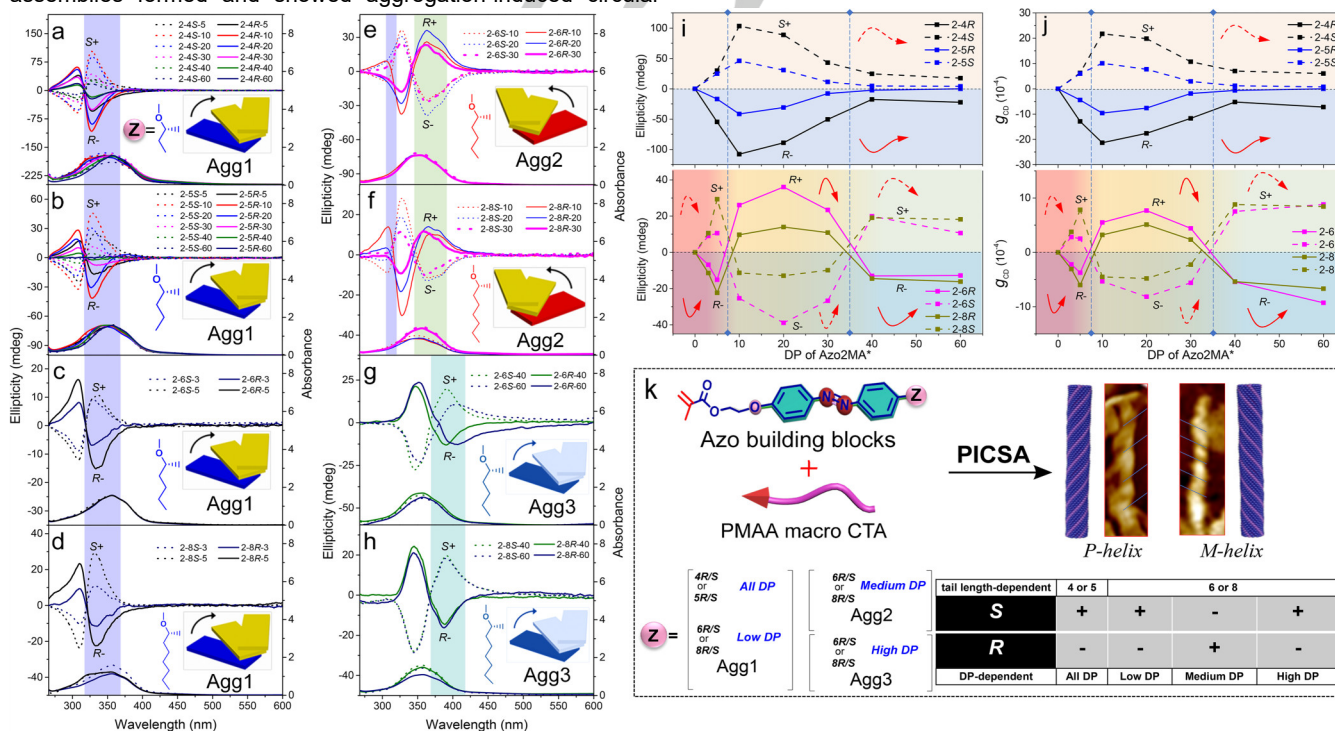


Figure 1. CD and UV-vis spectra of a) 2-4*R/S* and b) 2-5*R/S* with different DP of Azo blocks; c) 2-6*R/S* and d) 2-8*R/S* with DP = 3, 5; e) 2-6*R/S* and f) 2-8*R/S* with DP = 10, 20, 30; g) 2-6*R/S* and h) 2-8*R/S* with DP = 40, 60. The i) CD maximum and j) g_{CD} values of Azo-BCP supramolecular assemblies with different DP of Azo blocks (Kuhn's anisotropy, $g_{\text{CD}} = \Delta\epsilon/\epsilon = [\text{ellipticity}/32\ 980]/\text{absorbance}$ at the CD extremum). k) Tail length- and DP-dependent multiple chiroptical inversion.

Unexpectedly, as the DP of Azo blocks continued to increase (DP = 40, 60; Figures 1g and 1h), the bisignate Cotton bands were inverted again (Agg3). For this aggregation mode, *S*-type assemblies showed significant positive Cotton effects, whereas *R*-type assemblies exhibited negative effects. Meanwhile, the exciton coupling crossovers are mostly red-shifted and centered at ca. 367 nm, indicating a novel stacking mode significantly different from Agg1 (320 nm) and Agg2 (348 nm). The dependence of the CD maximum and g_{CD} values on the tail length and DP of Azo blocks were further analyzed in Figures 1i and 1j. For 2-4(5)*R/S* (2-4*R/S* and 2-5*R/S*), CD and g_{CD} values of both enantiomers are totally mirror-imaged, which increased gradually and then decreased with the increase of DP of Azo core-forming blocks, and no chiroptical inversion occurs. For 2-6(8)*R/S*, however, the CD and g_{CD} values are inverted twice, essentially depending on the DP of Azo blocks. Taking 2-6*S* Azo assemblies as an example, the CD and g_{CD} values were both positive at low DP, but first increased and gradually decreased to nearly zero, and then inverting to negative values as the DP increased. Subsequently, the negative CD and g_{CD} values increased to the absolute maximum before reaching zero again. Finally, they were completely inverted to positive values at high DP. Comparing chiroptical properties among these assemblies, a unique tail length-dependent chiroptical inversion effect was found. Polymers 2-4(5)*R/S* with shorter alkyl chains showed a single mirrored signal. In contrast, polymers 2-6(8)*R/S* with longer tails showed multiple chiroptical inversion behavior depending on DP of Azo blocks. As a result, the chiroptical properties of Azo-BCP assemblies can be controlled by tail length modification and in-situ DP variation during polymerization, regardless of whether the molecular stereogenic center was the same (Figure 1k).

Generally, the handedness of helical nanostructures is highly determined by the molecular chirality.^[1a] In this study, however, modulating tail length and DP of Azo blocks drive the morphological change and helix-to-helix transition between *P*- and *M*-helix (right-handed, *P*; left-handed, *M*), which is not solely dependent on single molecular configuration (Figure 2a). With the increase of DP, the morphology may be change for minimizing the energetically unfavorable hydrophobe-solvent interactions. For Azo-polymers 2-4(5)*R/S*, the morphology gradually changed from irregular nanofibers to micelles with the DP of Azo blocks increased (Figures 2b and S8). For Azo-polymers 2-6(8)*R/S*, the well-defined nanowires were built in a wide range of Azo block lengths (Figures 2c and S9). The nanowires were further characterized by atomic force microscopy (AFM). Taking 2-8*S* as an example (Figures 2d and S9), only short nanowires (Agg1) with several nanometers in height were observed when the DP of Azo blocks is less than 5. As the DP increased (10, 20, 30), the nanowires of Agg2 lead to *M*-type helix, whereas the nanowires of Agg3 with high DP (40, 60) present helical nanowires with *P*-helicity. In comparison with 2-8*S*, the morphologies of 2-8*R* changed from short nanowires to *P*-helicity and then to opposite *M*-helicity with the DP of Azo blocks increased, which is consistent with the opposite chiroptical properties from CD measurements. To the best of our knowledge, the twisted suprastructures with opposite screw sense are very rare to be directly observed in side-chain Azo-polymers. The tail length-dependent morphological transition can be due to the increased hydrophobe-solvent interactions, while the DP-dependent helicity inversion is probably driven by the transition of stacking modes in bistable LC phase (*vide infra*).

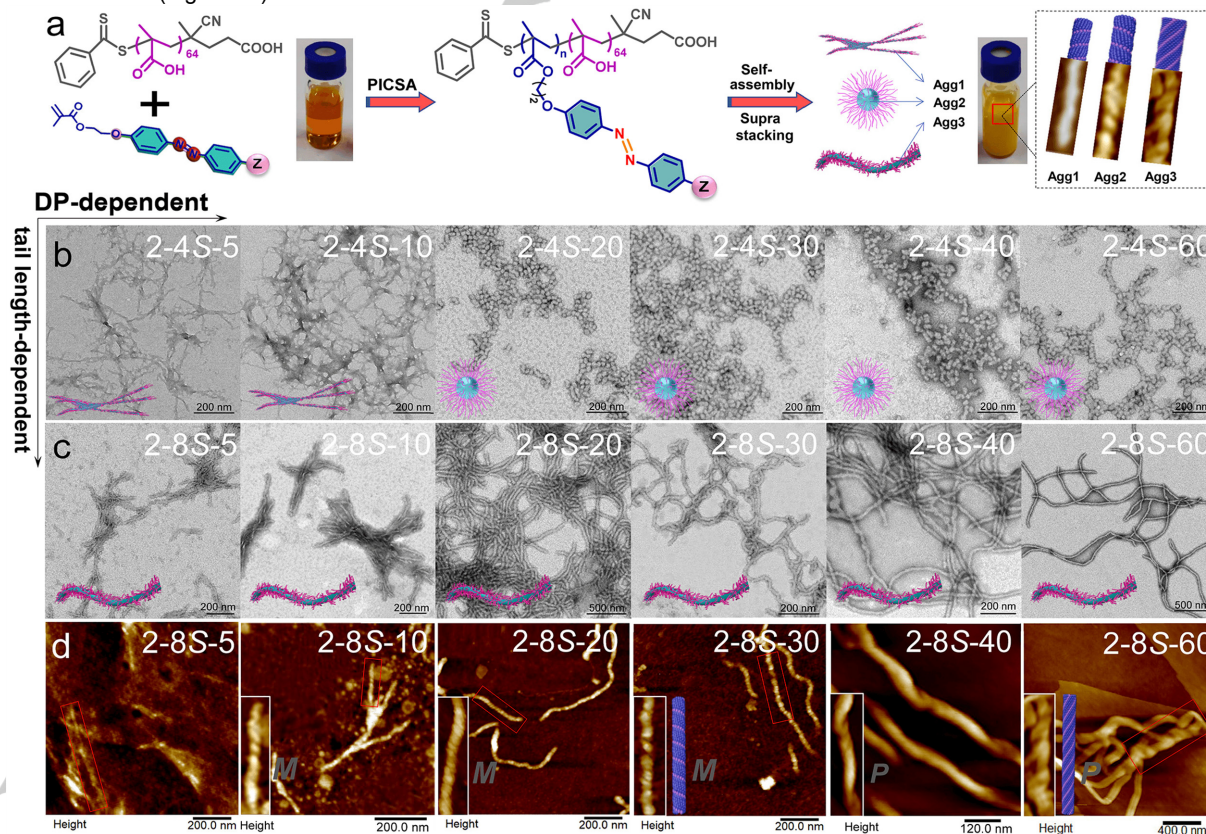


Figure 2. a) The helicity inversion and transition of Azo-BCP assemblies in PICSA process. TEM images of b) 2-4*S* and c) 2-8*S* Azo-BCP assemblies with different DP of Azo blocks. d) AFM images of the helical nanowires constructed by 2-8*S* Azo-BCPs.

The *trans-cis* isomerization of the Azo chromophores has been demonstrated to trigger the chiroptical response from *trans*-origin chiral aggregation to *cis*-origin achiral disaggregation.^[4b] Obviously, the nature of this chiroptical feature is the general “on-off” response, in which the chiroptical signals are changed between “on” and “off” states, without the involvement of the “inversion” response. Irradiating the Azo-BCP assemblies formed by PICSA process with 365 nm UV light caused a smooth decrease in π - π^* transition of *trans*-Azo in the range of 300–400 nm, accompanied by an increase in n - π^* transition of *cis*-Azo at 455 nm, regardless of the aggregation modes (Figures 3a, S10 and S11). Meanwhile, the CD amplitudes of the assemblies also decreased correspondingly with increasing irradiation time and completely disappeared at photostationary state (PSS), due to the formation of bent *cis*-form Azo units in polymer side chains. Compared with the time of Agg2 and Agg3 to reach PSS, Agg1 exhibited the highest degree of UV resistance (Figures 3b and 3c), indicating that the interactions within Agg1 are relatively stronger. It should be noted that these three aggregation modes exhibited mutually opposite chiroptical CD signals, so the Cotton effects of 2-6*R/S*-10 assemblies (containing Agg1 and Agg2) undergo a reversal in the process of UV light irradiation (red lines in Figure 3c). Interestingly, the Azo-BCP assemblies can recover its chiroptical signals with different pathway, by heating-cooling treatment (H-C) (Figures 3d and S12). The CD-silent Azo-BCP assemblies regained apparent CD intensity that increased with aging time, reaching a plateau after 15 min (Figures 3e, S12 and S13). Compared to the original CD sign, the sign of CD signals of Agg1 remained unchanged in 2-4(5)*R/S*, but transformed to multiple coupling (Agg1+Agg2) in 2-6(8)*R/S*. Meanwhile, the CD sign of Agg2 also maintained in 2-6(8)*R/S*; however, the CD sign of Agg3 disappeared completely and inverted to that similar to Agg2, accompanying by the blue-shifted exciton coupling center (Figure S12). These results indicate that the formation of stable Agg1 and Agg2 in PICSA process are thermodynamical pathways in polymers 2-4(5)*R/S* and 2-6(8)*R/S*, respectively; while the pathway to obtain Agg3 in polymers 2-6(8)*R/S* is kinetically controlled, forming a kinetically unstable Agg3-product.

The chiroptical switches were built by the *trans-cis-trans* isomerization of Azo chromophores and have almost no fatigue after 5 cycles of alternating UV light irradiation and H-C treatment (Figures S14 and S15). Moreover, the supramolecular chirality of the Azo-BCP assemblies can be purely controlled by thermal-stimulus. Upon heating the original Azo-BCP assemblies formed by PICSA, the CD intensity of the assemblies gradually attenuated with the increasing temperature, and disappeared at nearly 90 °C (Figures 3f and S16). The CD signals reappeared when the assemblies were gradually cooled to room temperature (Figures 3g and S16). The CD sign of thermodynamically stable Agg1 and Agg2 was retained in polymers 2-4(5)*R/S* and 2-6(8)*R/S*, respectively; while the CD sign of kinetically Agg3 in polymers 2-6(8)*R/S* is inverted to that similar to Agg2 (Figures S16 and S17). The results are similar to those observed after UV/H-C process, but the mechanism for chiroptical attenuation is different, which is attributed to the formation of bent *cis*-Azo units induced by UV light and non-associated *trans*-Azo units upon heating, respectively.

To unveil the mechanism of tail-length dependent chiroptical inversion phenomena, the mesomorphic properties and inner stacking modes of Azo-BCPs were investigated. As presented in Figure 4a, polymers 2-4(5)*R/S* (Agg1) are amorphous according

to the differential scanning calorimetry (DSC) results. Besides, no scattering peaks were detected by small-angle X-ray scattering (SAXS) in the angle region where LC structures are expected (Figure 4b and S18), and only broad peaks with a normal distribution ($2\theta = 16.0^\circ$) were observed in wide-angle X-ray diffraction (WAXD) patterns (Figure 4c and S18), also confirmed that they are amorphous without long-range ordered LC structures.

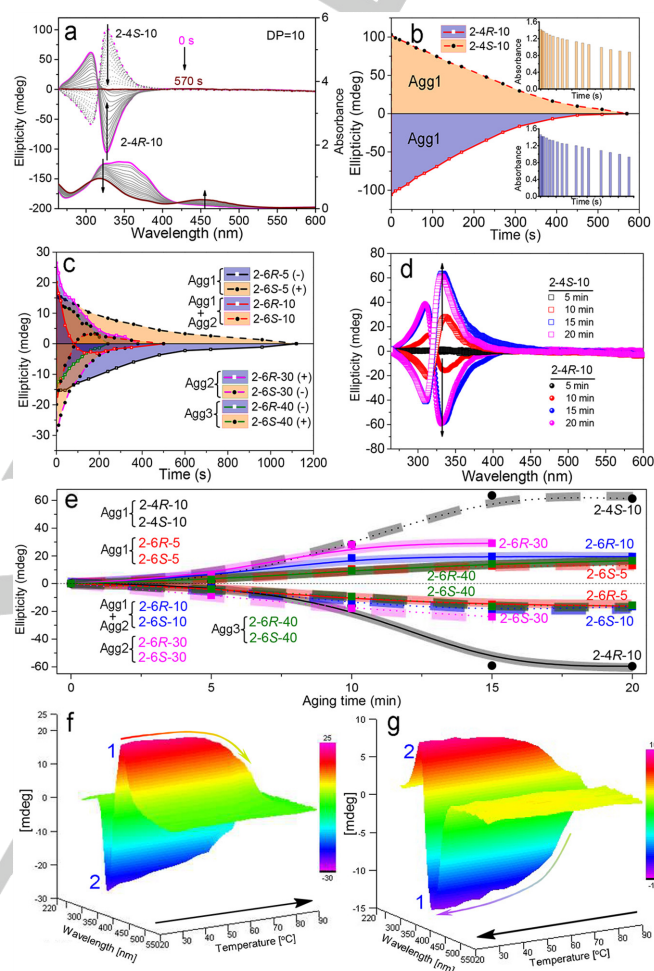


Figure 3. a) CD and UV-vis spectra of 2-4*R/S*-10 assemblies upon 365 nm light irradiation. b) Changes of the CD maximum and the corresponding absorption (insert) of 2-4*R/S*-10 assemblies at the first Cotton band (327.5 nm). c) The CD maximum of different aggregation modes upon 365 nm UV light irradiation. d) The CD spectral changes of 2-4*R/S*-10 assemblies upon H-C treatment. e) Aging time-dependent CD maximum of different aggregation modes represented by 2-4*R/S* and 2-6*R/S*. CD effect inversion of 2-6*S*-40 (Agg3) with f) increasing and g) decreasing temperature.

For polymers 2-6(8)*R/S* containing DP-dependent chirality/helix inversion, however, they clearly show the mesophase-isotropic phase transition T_i at 110–130 °C (Figure 4a). Meanwhile, polymers 2-6(8)*R/S* with low DP (5 for Agg1) exhibit amorphous phase, but they show clear diffraction peaks in WAXD patterns as the DP increased (30 for Agg2; 60 for Agg3), indicating the formation of LC phase structures (Figures 4c and S19). Two scattering peaks were observed in SAXS patterns in the small-angle regions ($q_2/q_1 = 2:1$, Figures 4b, S20 and S21), indicating a smectic phase with a layer spacing of about 4.45 nm (2-6*R/S*) and 4.76 nm (2-8*R/S*). Furthermore, the layer thickness did not vary with the temperature (Figure S22),

and is less than twice the fully extended chain length of the Azo side chain ($2L = 4.62$ nm for 2-6R/S and 4.94 nm for 2-8R/S, calculated by Gaussian 09, Figure S23). These results suggested an orthogonal smectic A phase (SmA^*) that has a double layered structure with interdigitation of the side chains. Interestingly, POM images indicated that homopolymers P6(8)R/S-30 exhibited a Twist Grain Boundary A^* phase with filament textures (TGBA*, a specific SmA^* phase with a cholesteric-like helical director field), whereas homopolymers P6(8)R/S-60 counterparts showed SmA^* phase with focal-conic textures (Figures 4d, 4e and S24), as assigned by Kozlovsky et al.^[23] The homopolymers P8R/S-30 films were transparent and weakly birefringent. Contrarily, the homopolymers P8R/S-60 films were more turbid and strongly birefringent at room temperature, indicating the DP-dependent biphasic LC behavior. Bright aggregated spots of 2-8R/S-60 Azo-BCPs also can be observed at room temperature (without thermal treatment), although they are difficult to melt to form an obvious texture due to strong hydrogen bonding in PMAA blocks (Figure S25).

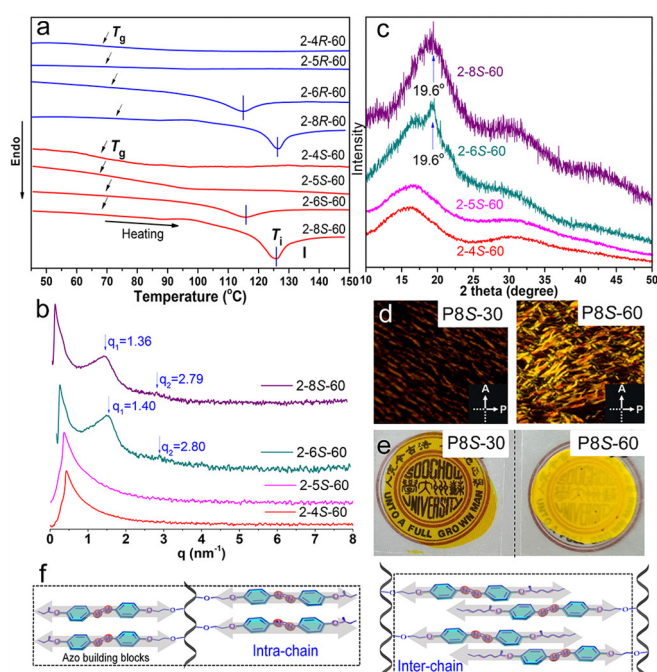


Figure 4. a) DSC curves of Azo-polymers with different tail lengths. b) SAXS patterns of amorphous 2-4(5)S-60 and smectic 2-6(8)S-60. c) WAXD profiles of amorphous 2-4(5)S-60 and smectic 2-6(8)S-60. d) POM images and e) photographs of transparent homopolymer P8S-30 and translucent homopolymer P8S-60. f) Schematic presentation of intra-chain and inter-chain stacking, the double arrow presents the polarization axis of Azo electronic transition.

Hence, the chirality of Agg1 exists in the non-LC phase, while the opposite chirality of Agg2 and Agg3 comes from the TGBA* and SmA^* phase, respectively. These mutually opposite chiroptical properties are the characteristics of exciton coupling between closely situated transition dipole moments on neighboring Azo units in chiral configurations. Most researchers concur that the single chiroptical properties in Azo-polymers are attributed to chiral H -aggregates.^[24] In this system, however, the chirality induced by Agg1 may originate from intra-chain interactions (π - π stacking), while the chirality effect of Agg2 and Agg3 comes from predominant inter-chain H - and J -aggregation of Azo mesogens (Figure 4f). First of all, the exciton coupling

crossovers of Agg2 and Agg3 are centered at ca. 348 nm and 367 nm, respectively. Accompanied by the changes in UV-vis absorption (Figure S26), the corresponding absorption shoulders located at 340 nm and 377 nm are hypsochromical (blue)-shifted and bathochromical (red)-shifted by ca. 17 nm and 20 nm in contrast to the main absorption (357 nm, isolated Azo) of dissolved polymers. These indicate that the chiral organization of Agg2 and Agg3 dominates with functionality-oriented inter-chain H - and J -aggregates in the LC domains. The shoulders are also observed in other Azo-BCP assemblies, exhibiting a DP-dependent balance (Figures S26c and S26d). Furthermore, an unexpected absorption band equivalent to the coupling center of Agg1 was observed at 320 nm, showing a larger blue shift of >35 nm compared to that of the isolated Azo chromophores (357 nm). Such a striking blue shift indicates that the aggregation mode of Agg1 is tighter than H -aggregation in consistence with the results of relatively high UV light-resistance. Due to the intra-chain interactions are more likely to occur in polymers 2-6(8)R/S-5 (with few repeating units), temperature-dependent decrease of circular dichroism and UV-vis absorption indicates that such packing mode is more likely to be π - π stacking between intra-chain coplanar Azo units (Figure S27). Theoretical simulations and calculations provide that the distance between intra-chain adjacent Azo units in chiral configuration is 3.6 Å (Figure S28, calculated by Gaussian 09), which is the typical distance of π - π stacking (3.5 Å) and smaller than that in mesogens packing organization (4.45 nm in 2-6R/S and 4.76 nm in 2-8R/S according to X-ray diffraction). Furthermore, reproducible Gaussian-typed peak analysis was obtained by fitting four peaks with local absorption maxima at ca. 320 nm for intra-chain π - π stacking, 340 nm for H -aggregation, 357.5 nm for non-associated chromophores and 377.5 nm for J -aggregation (Figure S29). The simulated intra-chain π - π stacking, H - and J -type modes was also optimized with a universal force field followed by Zerner's Intermediate Neglect of Differential Overlap (ZINDO) calculations (Figure S30). The mutually opposite bisignate electronic CD bands are derived from different stacking modes of helical structures and fully support the experimentally observed chiroptical inversion phenomena. As a result, the chirality of Agg1 is probably induced by the intra-chain π - π stacking in amorphous phase, while the chirality of Agg2 and Agg3 originates from H - and J -modes in TGBA* and SmA^* phase, respectively. The amorphous-to-LC phase transition and biphasic LC interconversion allow the transcription of three stacking modes, thereby controlling the dynamic reversal of supramolecular chirality (Figure S31).

In summary, for the first time, we have demonstrated the chiroptical control of side-chain Azo-polymer assemblies by the simple tail length modification and in-situ DP variation. The study also elucidated the mechanism of the thermodynamic chiroptical properties of Agg1 and Agg2, and the kinetics for Agg3 interconversion. The DP-, UV light-, temperature-, aging time-dependent chiroptical properties and LC characterization indicated that the length of their alkyl chains determines the amorphous-LC phase transition and appears to be the driving force for the chiroptical inversion. The chirality of amorphous Azo-polymers with short tails is induced by the intra-chain π - π stacking, while the multiple chiroptical inversion of Azo-polymers with long tails is significantly DP-dependent and probably triggered by the transition of dominated intra-chain π - π stacking

in amorphous state (low DP), *H*- and *J*-aggregation in TGBA* (medium DP) and Sma* (high DP) biphasic state, respectively. The chirality control and modulation of Azo-polymers will open a new gate to design and construct functional materials with the desired chiroptical properties.

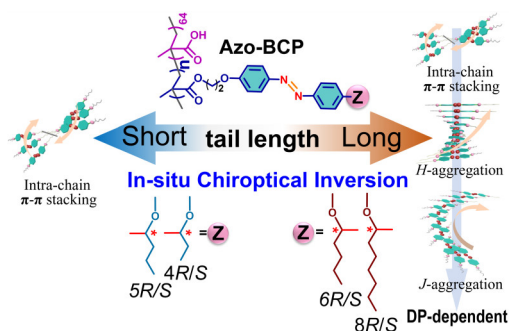
Acknowledgements

The authors are grateful for the financial support from the National Nature Science Foundation of China (92056111 and 21971180), Nature Science Key Basic Research of Jiangsu Province for Higher Education (No.19KJA360006), Postgraduate Research & Practice Innovation Program of Jiangsu Province (KYCX20_2655), the Priority Academic Program Development (PAPD) of Jiangsu Higher Education Institutions and the Program of Innovative Research Team of Soochow University.

Keywords: polymerization-induced self-assembly · azobenzene · supramolecular chirality · liquid-crystalline polymer

- [1] a) M. H. Liu, L. Zhang, T. Y. Wang, *Chem. Rev.* **2015**, *115*, 7304-7397; b) E. Yashima, N. Ousaka, D. Taura, K. Shimomura, T. Ikai, K. Maeda, *Chem. Rev.* **2016**, *116*, 13752-13990.
- [2] a) N. Suzuki, M. Fujiki, R. Kimpinde-Kalunga, J. R. Koe, *J. Am. Chem. Soc.* **2013**, *135*, 13073-13079; b) W. Q. Peng, M. Motonaga, J. R. Koe, *J. Am. Chem. Soc.* **2004**, *126*, 13822-13826.
- [3] a) M. M. Green, M. P. Reidy, R. J. Johnson, G. Darling, D. J. O'leary, G. Willson, *J. Am. Chem. Soc.* **1989**, *111*, 6452-6454; b) M. M. Green, N. C. Peterson, T. Sato, A. Teramoto, R. Cook, S. Lifson, *Science* **1995**, *268*, 1860-1866; c) Y. Nagata, T. Nishikawa, M. Sugimoto, *J. Am. Chem. Soc.* **2014**, *136*, 15901-15904.
- [4] a) S. I. Sakurai, K. Okoshi, J. Kumaki, E. Yashima, *J. Am. Chem. Soc.* **2006**, *128*, 5650-5651; b) W. Zhang, K. Yoshida, M. Fujiki, X. L. Zhu, *Macromolecules* **2011**, *44*, 5105-5111; c) K. Takaishi, K. Iwachido, T. Ema, *J. Am. Chem. Soc.* **2020**, *142*, 1774-1779.
- [5] a) H. K. Bisoyi, Q. Li, *Angew. Chem. Int. Ed.* **2016**, *55*, 2994-3010; b) L. B. Wang, L. Yin, W. Zhang, X. L. Zhu, M. Fujiki, *J. Am. Chem. Soc.* **2017**, *139*, 13218-13226; c) H. J. Jiang, Y. Q. Jiang, J. L. Han, L. Zhang, M. H. Liu, *Angew. Chem. Int. Ed.* **2019**, *58*, 785-790.
- [6] a) E. Yashima, K. Maeda, Y. Okamoto, *Nature* **1999**, *399*, 449-451; b) H. Goto, E. Yashima, *J. Am. Chem. Soc.* **2002**, *124*, 7943-7949; c) G. F. Liu, L. Y. Zhu, W. Ji, C. L. Feng, Z. X. Wei, *Angew. Chem. Int. Ed.* **2016**, *55*, 2411-2415.
- [7] a) J. del Barrio, R. M. Tejedor, L. Oriol, *Eur. Polym. J.* **2012**, *48*, 384-390; b) J. del Barrio, R. M. Tejedor, L. S. Chinelatto, C. Sanchez, M. Pinol, L. Oriol, *J. Mater. Chem.* **2009**, *19*, 4922-4930.
- [8] a) Z. Lv, Z. Chen, K. Shao, G. Qing, T. Sun, *Polymers* **2016**, *8*, 310; b) K. Bauri, S. Pant, S. G. Roy, P. De, *Polym. Chem.* **2013**, *4*, 4052-4060.
- [9] a) S. Cantekin, D. W. Balkenende, M. M. Smulders, A. R. Palmans, E. W. Meijer, *Nat. Chem.* **2011**, *3*, 42-46; b) Y. Yan, K. Deng, Z. Yu, Z. X. Wei, *Angew. Chem. Int. Ed.* **2009**, *48*, 2003-2006.
- [10] a) S. Ogi, T. Fukui, M. L. Jue, M. Takeuchi, K. Sugiyasu, *Angew. Chem. Int. Ed.* **2014**, *53*, 14363-14367; b) G. Liu, J. Sheng, H. Wu, C. Yang, G. Yang, Y. Li, R. Ganguly, L. Zhu, Y. Zhao, *J. Am. Chem. Soc.* **2018**, *140*, 6467-6473; c) S. Yagai, T. Seki, T. Karatsu, A. Kitamura, F. Wurthner, *Angew. Chem. Int. Ed.* **2008**, *47*, 3367-3371.
- [11] a) T. Nakano, Y. Okamoto, *Chem. Rev.* **2001**, *101*, 4013-4038; b) O. Ikkala, G. ten Brinke, *Science* **2002**, *295*, 2407-2409; c) S. Cai, J. Chen, S. Wang, J. Zhang, X. Wan, *Angew. Chem. Int. Ed.* **2021**, *60*, 9686-9692.
- [12] a) M. Douverne, Y. Ning, A. Tatani, F. C. Meldrum, S. P. Armes, *Angew. Chem. Int. Ed.* **2019**, *58*, 8692-8697; b) R. H. Deng, M. J. Derry, C. J. Mable, Y. Ning, S. P. Armes, *J. Am. Chem. Soc.* **2017**, *139*, 7616-7623.
- [13] a) S. H. Xu, J. Yeow, C. Boyer, *ACS Macro Lett.* **2018**, *7*, 1376-1382; b) J. Yeow, C. Boyer, *Adv. Sci.* **2017**, *4*, 1700137.
- [14] a) G. H. Zheng, C. Y. Pan, *Macromolecules* **2006**, *39*, 95-102; b) J. M. Zhou, C. Y. Hong, C. Y. Pan, *Mater. Chem. Front.* **2017**, *1*, 1200-1206.
- [15] a) S. Guan, A. H. Chen, *Macromolecules* **2020**, *53*, 6235-6245; b) S. Guan, W. Wen, Z. Z. Yang, A. H. Chen, *Macromolecules* **2020**, *53*, 465-472.
- [16] a) B. H. Zhang, X. Q. Lv, A. Q. Zhu, J. W. Zheng, Y. Q. Yang, Z. S. An, *Macromolecules* **2018**, *51*, 2776-2784; b) F. Lv, Z. S. An, P. Y. Wu, *Nat. Commun.* **2019**, *10*, 1397.
- [17] a) S. Jimaja, S. Varlas, Y. Xie, J. C. Foster, D. Taton, A. P. Dove, R. K. O'Reilly, *ACS Macro Lett.* **2020**, *9*, 226-232; b) J. Chen, S. Cai, R. Wang, S. Wang, J. Zhang, X. Wan, *Macromolecules* **2020**, *53*, 1638-1644.
- [18] X. X. Cheng, T. F. Miao, L. Yin, Y. J. Ji, Y. Y. Li, Z. B. Zhang, W. Zhang, X. L. Zhu, *Angew. Chem. Int. Ed.* **2020**, *59*, 9669-9677.
- [19] L. Chen, X. F. Li, Q. Yan, *Macromolecules* **2021**, *54*, 5077-5086.
- [20] a) X. Tong, L. Cui, Y. Zhao, *Macromolecules* **2004**, *37*, 3101-3112; b) S. Iamsaard, S. J. Asshoff, B. Matt, T. Kudernac, J. J. L. M. Cornelissen, S. P. Fletcher, N. Katsonis, *Nat. Chem.* **2014**, *6*, 229-235; c) J. A. Lv, Y. Y. Liu, J. Wei, E. Q. Chen, L. Qin, Y. L. Yu, *Nature* **2016**, *537*, 179-184.
- [21] a) S. Huang, Y. X. Chen, S. D. Ma, H. F. Yu, *Angew. Chem. Int. Ed.* **2018**, *57*, 12524-12528; b) L. Yin, T. F. Miao, X. X. Cheng, Z. C. Jiang, X. Tong, W. Zhang, Y. Zhao, *ACS Macro Lett.* **2021**, *10*, 690-696; c) J. N. Yuan, X. M. Lu, Q. X. Li, Z. G. Lu, Q. H. Lu, *Angew. Chem. Int. Ed.* **2021**, *60*, 12308-12312.
- [22] X. X. Cheng, T. F. Miao, Y. L. Qian, Z. B. Zhang, W. Zhang, X. L. Zhu, *Int. J. Mol. Sci.* **2020**, *21*, 6186.
- [23] a) M. Kozlovsky, B. J. Jungnickel, H. Ehrenberg, *Macromolecules* **2005**, *38*, 2729-2738; b) J. W. Goodby, M. A. Waugh, S. M. Stein, E. Chin, R. Pindak, J. S. Patel, *Nature* **1989**, *337*, 449-452; c) G. Iftime, F. L. Labarthe, A. Natansohn, P. Rochon, *J. Am. Chem. Soc.* **2000**, *122*, 12646-12650.
- [24] a) R. M. Tejedor, L. Oriol, J. L. Serrano, F. P. Urena, J. J. L. Gonzalez, *Adv. Funct. Mater.* **2007**, *17*, 3486-3492; b) S. W. Choi, S. Kawauchi, N. Y. Ha, H. Takezoe, *Phys. Chem. Chem. Phys.* **2007**, *9*, 3671-3681; c) Y. L. Wu, A. Natansohn, P. Rochon, *Macromolecules* **2004**, *37*, 6801-6805.

Entry for the Table of Contents



The multiple chiroptical inversion in Azo biphasic liquid-crystalline polymers is firstly realized in-situ by the tail length modification and DP variation. The amorphous-to-LC phase transition and biphasic LC interconversion allow the transcription of three stacking modes, thereby controlling the dynamic reversal of supramolecular chirality.